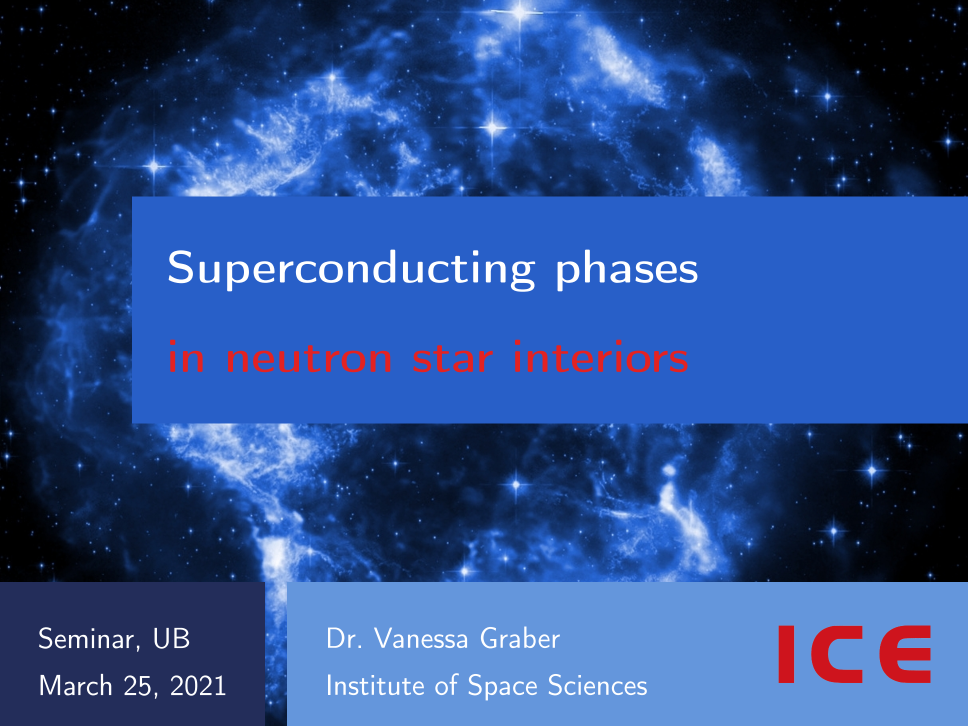

Superconducting phases in neutron star interiors

Seminar, UB
March 25, 2021

Dr. Vanessa Graber
Institute of Space Sciences

Contents

1 Neutron Stars in a Nutshell

2 Background on Superconductivity

3 Microscale Neutron Star Model

Contents

1 Neutron Stars in a Nutshell

2 Background on Superconductivity

3 Microscale Neutron Star Model

Neutron Stars

Formation

- Neutron stars are one type of **compact remnant**, created during the final stages of stellar evolution.
- When a massive star of $\sim 8 - 30\,M_\odot$ runs out of fuel, it collapses under its own gravitational attraction and explodes in a **supernova**.
- During collapse, **electron captures** $(p + e^- \rightarrow n + \nu_e)$ produce neutrons.
- NS have radii between $9 - 13\,\mathrm{km}$ and weigh $1.2 - 2.2\,M_\odot$, resulting in densities up to $\rho \simeq 10^{15}\,\mathrm{g\,cm^{-3}}$.

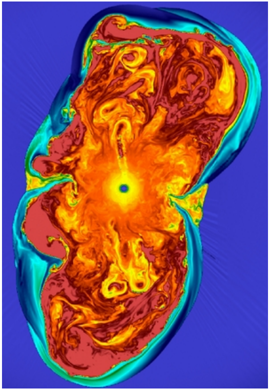

Figure 1: Snapshot of 3D core-collapse supernova simulation (Mösta et al., 2014).

Neutron Stars Structure

- The interior structure is complex and influenced by the (unknown) equation of state. However, there is a **canonical understanding**.
- After $\sim 10^4$ years neutron stars are in equilibrium and have temperatures of $10^6 - 10^8\,\mathrm{K}$. They are composed of **distinct layers**.
- For our purposes, we separate neutron stars into a **solid crust** and a **fluid core**, containing three distinct superfluid components.

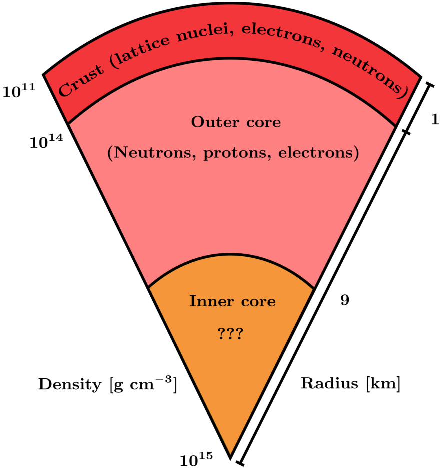
Crust (lattice nuclei, electrons, neutrons)
Outer core
(Neutrons, protons, electrons)
Inner core
???
10^{11}
10^{14}
10^{15}
Density [g cm^{-3}]
1
9
Radius [km]

Figure 2: Sketch of the neutron star interior.

Quantum condensates

- Neutron stars are hot compared to low-temperature experiments on Earth, but cold in terms of their nuclear physics (Migdal, 1959).
- Neutrons and protons are **fermions** and can become unstable to **Cooper pair formation** due to an attractive contribution to the nucleon-nucleon interaction potential.
- The pairing process is typically described within the microscopic **BCS** theory of superconductivity (Bardeen, Cooper & Schrieffer, 1957).
- Compare the equilibrium to the nucleons' **Fermi temperature**:

$$T_{\mathrm{F}} = k_{\mathrm{B}}^{-1} E_{\mathrm{F}} \sim 10^{12}\,\mathrm{K} \gg 10^{6} - 10^{8}\,\mathrm{K}. \tag{1}$$

Neutron star matter is strongly influenced by quantum mechanics!

Transition temperatures

- Detailed BCS calculations provide the pairing gaps Δ, which are associated with the **critical temperatures** T_c for the superfluid and superconducting phase transitions.

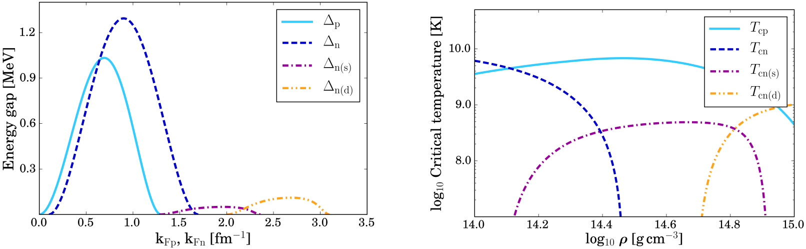

Figure 3: Left: Parametrised proton (singlet) and neutron (singlet, triplet) energy gaps as a function of Fermi wave numbers (Ho, Glampedakis & Andersson, 2012). Right: Critical temperatures of superconductivity/superfluidity as a function of the neutron star density. The values are computed for the NRAPR equation of state (Steiner et al., 2005; Chamel, 2008).

Contents

1 Neutron Stars in a Nutshell

2 Background on Superconductivity

3 Microscale Neutron Star Model

SC Background

A few basics

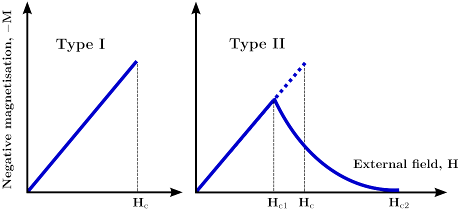

Figure 4: Magnetisation curves for a type-I (left) and type-II (right) medium with the same H_c.

- Superconductors are materials characterised by **vanishing electrical resistance** (perfect conductors) and **expulsion of magnetic flux**.

- They are often studied by their **response to an external field** H, providing information about the **internal magnetisation**. Due to their distinct responses, we historically distinguish **type-I** and **type-II media**.

- Many superconductor features close to the transition temperature are well described with the phenomenological **Ginzburg–Landau model**.

SC Background

The (old) type-II picture

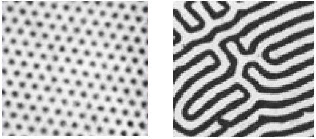

Figure 5: Type-II and intermediate type-I state (Brandt & Essmann, 1987).

- Due to high conductivity, the magnetic flux cannot be expelled from their interiors ⇒ neutron stars do not exhibit Meissner effect and are in a **metastable** state (Baym, Pethick & Pines, 1969; Ho, Andersson & Graber, 2017).

- State depends on **characteristic lengthscales** and standard considerations give $\kappa = \lambda_\star / \xi_{\rm ft} > 1/\sqrt{2}$ in the outer core, i.e., a **type-II state** with

$$H_{\rm c1} = 4\pi \mathcal{E}_{\rm ft} / \phi_0 \sim 10^{14}\,{\rm G}, \qquad H_{\rm c2} = \phi_0 / (2\pi \xi_{\rm ft}^2) \sim 10^{15}\,{\rm G}. \tag{2}$$

- Each fluxtube carries a **flux quantum** $\phi_0 = hc/2e \approx 2.1 \times 10^{-7}\,{\rm G\,cm}^2$. All flux quanta add up to the total magnetic flux, so that the **averaged magnetic induction** is related to the fluxtube area density $\mathcal{N}_{\rm ft}$:

$$B = \mathcal{N}_{\rm ft} \phi_0, \quad \rightarrow \quad \mathcal{N}_{\rm ft} \approx 4.8 \times 10^{18} \, \left(B / 10^{12}\,{\rm G} \right) {\rm cm}^{-2}. \tag{3}$$

Induction equation

- **Magnetic field evolution** in the outer core should be related to the mechanisms affecting the fluxtubes' motion, but these are rather poorly understood (Muslimov & Tsygan, 1985; Graber, 2017, e.g.).

- It is possible to use techniques of classical magnetohydrodynamics to derive a **superconducting induction equation** (Graber et al., 2015). For the standard coupling mechanism (electron scattering), one finds:

$$\partial_t B^i \approx \epsilon^{ijk} \nabla_j \left[\epsilon_{klm} v_{\rm p}^l B^m - \frac{\kappa B}{2\pi} \frac{m}{m_{\rm p}^*} \left(\mathcal{B}' \hat{B}^l \nabla_l \hat{B}_k + \mathcal{B} \epsilon_{klm} \hat{B}^l \hat{B}^s \nabla_s \hat{B}^m \right) \right], \quad (4)$$

  with inertial, conservative (Hall-like) and dissipative (Ohmic-like) term.

- The corresponding **timescales** are too slow to drive field evolution on observable timescales, i.e., $\tau_{\rm diss} \approx 10^9$ yrs and $\tau_{\rm cons} \approx 10^{11}$ yrs.

Contents

1 Neutron Stars in a Nutshell

2 Background on Superconductivity

3 Microscale Neutron Star Model

Motivation

- Our understanding of **macroscopic NS superconductivity** is mainly based on **time-independent equilibrium** and **single-component** considerations.
- It is unclear what happens in the **stellar interior at different densities** as the star cools below T_c and when **entrainment** is included ⇒ how can we better understand the **SC phase** and its formation?
- Focus on the **two-condensate aspect** and expand on **earlier works** by Alpar, Langer & Sauls (1984); Charbonneau & Zhitnitsky (2007); Alford & Good (2008); Haber & Schmitt (2017); see also Kobyakov (2020).

Wood, Graber & Newton (2020): Employ techniques for laboratory systems to construct **phase diagrams** by deducing the protons' ground state in presence of a magnetic field as a function of density.

Micro model

Galilean invariant GL model

- With entrainment, **velocity-dependent terms** in energy density read

$$F_{\mathsf{vel}} = \tfrac{1}{2}\rho_{\mathrm{p}}|\mathbf{V}_{\mathrm{p}}|^2 + \tfrac{1}{2}\rho_{\mathrm{n}}|\mathbf{V}_{\mathrm{n}}|^2 - \tfrac{1}{2}\rho^{\mathrm{pn}}|\mathbf{V}_{\mathrm{p}} - \mathbf{V}_{\mathrm{n}}|^2 \,, \qquad (5)$$

where ρ_{p} and ρ_{n} are the true mass densities, the coefficient $\rho^{\mathrm{pn}} < 0$ determines the strength of entrainment (Andreev & Bashkin, 1975) and $\mathbf{V}_{\mathrm{p,n}}$ are superfluid velocities related to canonical momenta, i.e., $\propto \nabla \arg \psi_{\mathrm{x}}$.

- In a mean-field framework, entrainment first enters at 4th order in $\psi_{\mathrm{n,p}}$ and 2nd order in their derivatives, i.e., we require a linear combination of

$$|\psi_x|^2|\boldsymbol{\nabla}\psi_y|^2,\ \psi_x\psi_y\boldsymbol{\nabla}\psi_x^\star\cdot\boldsymbol{\nabla}\psi_y^\star,\ \psi_x\psi_y^\star\boldsymbol{\nabla}\psi_x^\star\cdot\boldsymbol{\nabla}\psi_y,\ \psi_x^\star\psi_y^\star\boldsymbol{\nabla}\psi_x\cdot\boldsymbol{\nabla}\psi_y, \qquad (6)$$

where $x, y \in \{\mathrm{p}, \mathrm{n}\}$. Galilean invariance can be used to simplify the sum and is crucial to link our energy density to **nuclear physics models**.

Micro model

Helmholtz free energy density

- Total Helmholtz free energy density is obtained by adding entrainment terms to the usual free energy of a two-component superconductor, and introducing the magnetic vector potential **A** by **minimal coupling**:

$$
\begin{aligned}
F[\psi_\mathrm{p},\psi_\mathrm{n},\mathbf{A}] = {} & F_0 - \mu_\mathrm{p}|\psi_\mathrm{p}|^2 - \mu_\mathrm{n}|\psi_\mathrm{n}|^2 + \frac{g_\mathrm{pp}}{2}|\psi_\mathrm{p}|^4 + \frac{g_\mathrm{nn}}{2}|\psi_\mathrm{n}|^4 + g_\mathrm{pn}|\psi_\mathrm{p}|^2|\psi_\mathrm{n}|^2 \\
& + \frac{\hbar^2}{4m_\mathrm{u}}\left|\left(\boldsymbol{\nabla} - \frac{2ie}{\hbar c}\mathbf{A}\right)\psi_\mathrm{p}\right|^2 + \frac{\hbar^2}{4m_\mathrm{u}}|\boldsymbol{\nabla}\psi_\mathrm{n}|^2 + \frac{1}{8\pi}|\boldsymbol{\nabla}\times\mathbf{A}|^2 \\
& + h_1\left|\left(\boldsymbol{\nabla} - \frac{2ie}{\hbar c}\mathbf{A}\right)(\psi_\mathrm{n}^\star\psi_\mathrm{p})\right|^2 + \tfrac{1}{2}(h_2 - h_1)\boldsymbol{\nabla}(|\psi_\mathrm{p}|^2)\cdot\boldsymbol{\nabla}(|\psi_\mathrm{n}|^2) \\
& + \tfrac{1}{4}h_3\left(\left|\boldsymbol{\nabla}(|\psi_\mathrm{p}|^2)\right|^2 + \left|\boldsymbol{\nabla}(|\psi_\mathrm{n}|^2)\right|^2\right), \qquad (7)
\end{aligned}
$$

where F_0 is an arbitrary reference level and proton Cooper pairs have charge $2\mathrm{e}$. μ_p and μ_n are the chemical potentials, while g_pp and g_nn define the self-repulsion of the condensates, and g_pn their mutual repulsion.

Skyrme connection

- We use the full **Skyrme model** to determine the **stellar composition** (solving for baryon conservation, charge neutrality, beta equilibrium and equilibrium due to weak processes) (Chamel, 2008) but a separate **SF/SC gap parametrisation** (Andersson, Comer & Glampedakis, 2005; Ho et al., 2015).

- We also connect the Skyrme interaction to our energy functional to obtain **coefficients** h_i that allow a **realistic description** of the stellar interior:

$$h_1 = C_0^{\tau} - C_1^{\tau}\,, \qquad h_2 = -4C_0^{\Delta\rho} + 4C_1^{\Delta\rho}\,, \tag{8}$$

$$h_3 = h_4 = C_0^{\tau} + C_1^{\tau} - 4C_0^{\Delta\rho} - 4C_1^{\Delta\rho}\,. \tag{9}$$

- The parameter h_1 controls the **entrainment** (Chamel & Haensel, 2006)

$$\rho^{\mathrm{pn}} = -\frac{2}{\hbar^2} h_1 \rho_{\mathrm{n}} \rho_{\mathrm{p}}. \tag{10}$$

Micro model

Two thought experiments

- To find the **ground state** in the presence of an **imposed magnetic field**, we can control (i) the magnetic flux density, $\mathbf{B} = \nabla \times \mathbf{A}$, by imposing a mean flux $\overline{B}$, or (ii) the thermodynamic external magnetic field $\mathbf{H}$.

- Case (i) approximates the **neutron star interior**, which becomes superconducting as the star cools in the presence of a pre-existing field.

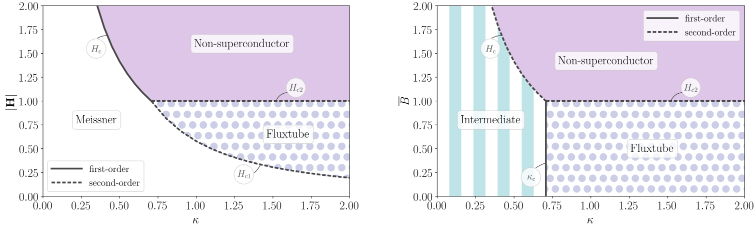

Figure 6: Phase diagrams for a one-component superconductor, for different values of the Ginzburg-Landau parameter, κ. The experiment with an imposed external field, $|\mathbf{H}|$, in nondimensional units is shown on the left, while the right panel shows the phase transitions in the experiment with an imposed mean flux, $\overline{B}$.

Micro model

Energy per flux quantum

- We solve the Euler-Lagrange equations with **quasi-periodic boundary conditions** (Wood et al., 2019), which involves specifying the domain size $L_x \times L_y$, and the number N of magnetic flux quanta within the domain $\Rightarrow$ different choices allow comparing **square** and **hexagonal lattices**.

- The Helmholtz free energy per magnetic flux quantum per unit length is

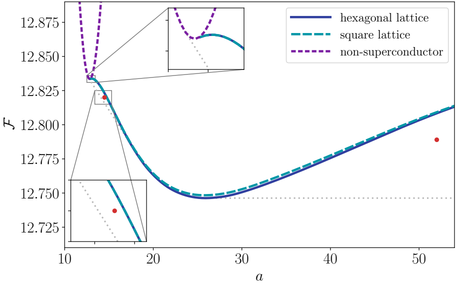

$$\mathcal{F} \equiv \frac{1}{N}\int_{x=0}^{L_x}\int_{y=0}^{L_y} F\,\mathrm{d}x\,\mathrm{d}y\,. \tag{11}$$

Figure 7: Helmholtz free energy per flux quantum per unit length, $\mathcal{F}$, as a function of the area per magnetic flux quantum, $a = 2\pi/\overline{B}$, for the NRAPR EoS at $n_{\mathrm{b}} = 0.2831/\mathrm{fm}^{3}$. The energy in the square (long-dashed, cyan) and hexagonal (solid, blue) lattice states matches smoothly onto the energy of the non-superconducting state (short-dashed, purple) at $a \simeq 12.9$.

Inhomogeneous ground states

- Choosing a sufficiently large domain, and values of a, we obtain examples of **inhomogeneous ground states** $\Rightarrow$ for NRAPR at $n_{\rm b} = 0.2831/{\rm fm}^3$ with $a = 14.5$ plus $N = 24$ (left) and $a = 52$ plus $N = 14$ (right).

- In both cases, the aspect ratio is $\sqrt{3}$ and the **pure hexagonal lattice** a possible state but not the ground state $\Rightarrow \mathcal{F}$ is lower than for pure lattice.

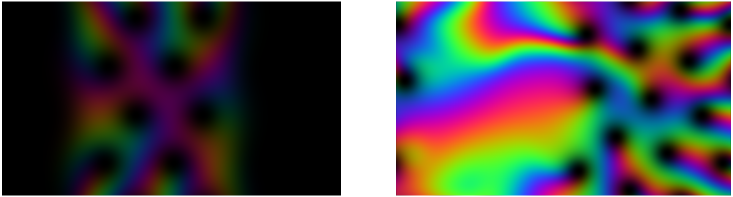

Figure 8: Inhomogeneous ground states for NRAPR. Brightness and hue indicate density and phase of the proton order parameter, $\psi_{\rm p}$, respectively. The left panel shows a mixture of non-superconducting protons and hexagonal fluxtube lattice, while the right one is mixture of Meissner state and hexagonal fluxtube lattice.

Micro model

Phase diagrams LNS

- When such mixed states are present, second-order phase transitions are replaced by **first-order transitions** at $H_{c1'} < H_{c1}$ and $H_{c2'} > H_{c2}$.
- We can determine **critical fields** (partially semi-analytically, partially numerically) and construct phase-diagrams of the superconducting state throughout the neutron star core. For the **LNS** equation of state:

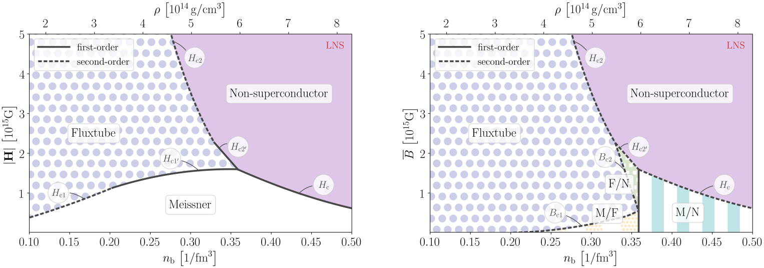

Figure 9: Phase diagrams for LNS. There are inhomogeneous regimes of the Meissner/Non-superconducting (M/N), Meissner/Fluxtube (M/F) and Fluxtube/Non-superconducting (F/N) states.

Micro model

NRAPR, SLy4, SQMC700

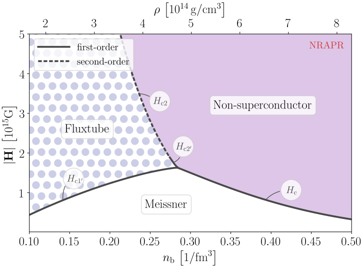

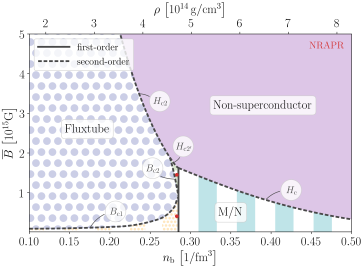

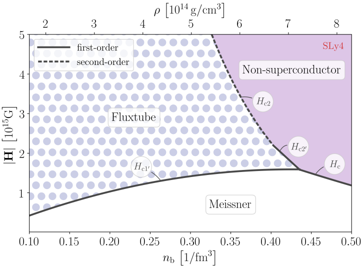

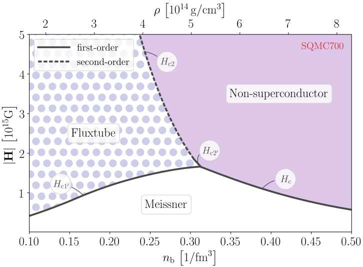

Micro model

Ska35s20, Skχ450

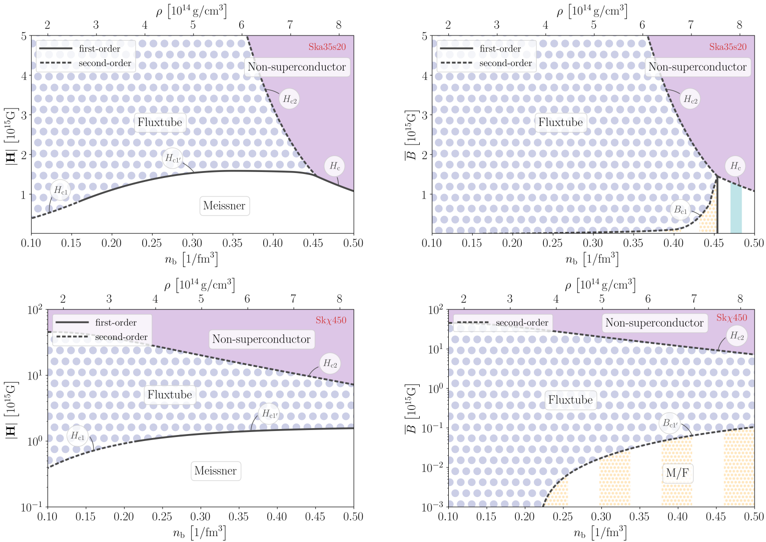

Micro model

Implications

- Entrainment causes **type-1.5 SC** due to fluxtube repulsion on short scales and attraction on large scales ⇒ when imposing $\overline{B}$, mixed states appear.
- For typical EoSs, the outer core of pulsars with $\lesssim 10^{14}$ G is not a type-II superconductor but mainly a type-1.5 system, where **magnetic flux is irregularly distributed** and **retained**.
- In the inner core, flux is distributed in an **intermediate type-I state**. The transition can be estimated via:

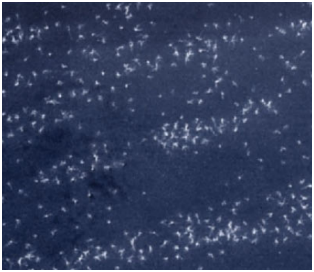

Figure 10: Magnetic decoration image of multi-band superconductor Mg2B (Moshchalkov et al., 2009).

$$\boxed{\frac{\lambda_\star}{\xi_{\rm ft}} = \frac{1}{\sqrt{2}}\sqrt{1 + h_1\,\frac{n_{\rm n}}{n_{\rm p}}}.} \qquad (12)$$

Flux distribution

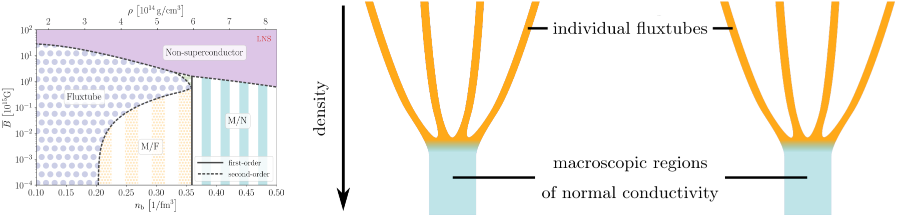

Figure 11: Zoomed-out version of the LNS phase diagram for a fixed mean flux (left). Schematic representation of the magnetic flux at the transition from outer to inner core (right).

- At low densities, protons are in a **type-1.5 regime**, where flux is quantized into thin fluxtubes (orange) of preferred separation (overall confined to a small fraction of the total volume).
- In the **type-I inner core**, flux is contained in macroscopic regions of normal conductivity (light blue) that alternate with flux-free regions.

Micro model

Caveats

- We assume that the **Skyrme model** correctly describes interactions up to the neutron star centre. If exotic particles / non-nucleonic matter are present, this would modify the picture at high densities.

- Our **superfluid gap models** (p: CCDK, n: TToa) are motivated by cooling observations of the Cas A supernova remnant but inconsistent with the mean-field description of the interacting particles.

- Our Ginzburg–Landau model is **time-independent** and neglects **rotation**, i.e., we do not capture dynamics or incorporate neutron vortices *yet*, which are crucial to get the full macroscopic picture.

- For a full dynamical model, we would need to incorporate the **normal electron component**. We do not have the formalism to consistently include such a (particle) component in the Ginzburg–Landau model *yet*.

Conclusions

- Neutron stars contain (at least) **three superfluids** that influence the stars' macroscopic properties. Theoretical modelling is difficult ⇒ use **laboratory counterparts** to understand them better.

- We use a **phenomenological two-component Ginzburg–Landau model** and connect it to the Skyrme interaction to determine the protons' ground state throughout the neutron star core ⇒ **inhomogeneous flux distributions** exist in most of the core.

- **Magnetic field evolution** in the core is poorly understood but crucial to explain observed field changes in pulsars (Narayan & Ostriker, 1990), the high activity of magnetars (Thompson & Duncan, 1995), or neutron star 'metamorphosis' (Viganò et al., 2013) ⇒ to **develop macroscopic models** we need to better understand microphysics.

The end

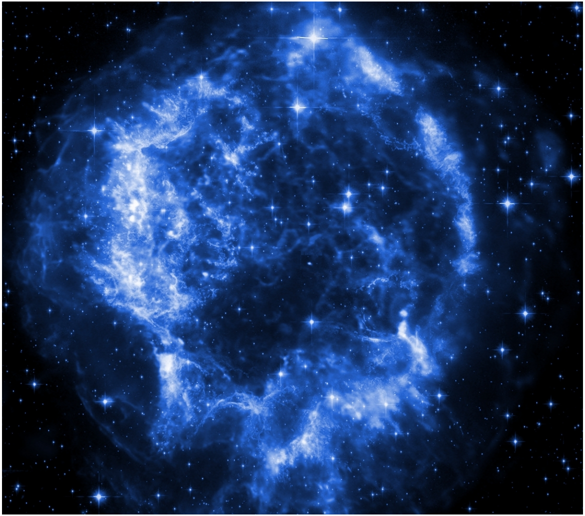

Appendix

Thought experiments

- To find the **ground state** for our system in the presence of an **imposed magnetic field**, we can perform two distinct experiments: we control (i) the magnetic flux density, $\mathbf{B} = \boldsymbol{\nabla} \times \mathbf{A}$, by imposing a mean or net magnetic flux, or (ii) the thermodynamic external magnetic field, $\mathbf{H}$.

- In the first case, we minimise the **Helmholtz free energy**, $\mathcal{F} = \langle F \rangle$, where the angled brackets represent some kind of integral over our physical domain $\Rightarrow$ closely approximates the conditions in the neutron star core, which becomes superconducting as the star cools in the presence of pre-existing magnetic field. The ground state can be **inhomogeneous**.

- In the second case, we minimise the dimensionless **Gibbs free energy**, $\mathcal{G} = \mathcal{F} - 2\kappa^2 \mathbf{H} \cdot \langle \mathbf{B} \rangle$. In an unbounded domain, the ground state is guaranteed to be **homogeneous**, and the phase diagram simpler.

Appendix

Euler-Lagrange equations

- Whether we work with $\mathcal{F}$ or $\mathcal{G}$, we obtain the same equations of motion:

$$\kappa^2 \boldsymbol{\nabla} \times (\boldsymbol{\nabla} \times \mathbf{A}) = \Im \left\{ \psi_\mathrm{p}^\star (\boldsymbol{\nabla} - \mathrm{i}\mathbf{A}) \psi_\mathrm{p} + \frac{h_1}{\epsilon} \psi_\mathrm{n} \psi_\mathrm{p}^\star (\boldsymbol{\nabla} - \mathrm{i}\mathbf{A})(\psi_\mathrm{n}^\star \psi_\mathrm{p}) \right\} , \quad (13)$$

$$\begin{aligned} \nabla^2 \psi_\mathrm{n} = {} & R^2 (|\psi_\mathrm{n}|^2 - 1)\psi_\mathrm{n} + \alpha (|\psi_\mathrm{p}|^2 - 1)\psi_\mathrm{n} \\ & - h_1 \psi_\mathrm{p} (\boldsymbol{\nabla} + \mathrm{i}\mathbf{A})^2 (\psi_\mathrm{p}^\star \psi_\mathrm{n}) \\ & - \psi_\mathrm{n} \nabla^2 \left(\frac{h_2 - h_1}{2} |\psi_\mathrm{p}|^2 + \frac{h_3}{2\epsilon} |\psi_\mathrm{n}|^2 \right) , \end{aligned} \quad (14)$$

$$\begin{aligned} (\boldsymbol{\nabla} - \mathrm{i}\mathbf{A})^2 \psi_\mathrm{p} = {} & (|\psi_\mathrm{p}|^2 - 1)\psi_\mathrm{p} + \frac{\alpha}{\epsilon} (|\psi_\mathrm{n}|^2 - 1)\psi_\mathrm{p} \\ & - \frac{h_1}{\epsilon} \psi_\mathrm{n} (\boldsymbol{\nabla} - \mathrm{i}\mathbf{A})^2 (\psi_\mathrm{n}^\star \psi_\mathrm{p}) \\ & - \psi_\mathrm{p} \nabla^2 \left(\frac{h_2 - h_1}{2\epsilon} |\psi_\mathrm{n}|^2 + \frac{h_3}{2} |\psi_\mathrm{p}|^2 \right) . \end{aligned} \quad (15)$$

Energy minimisation

- F is approximated numerically on a regular 2D grid. The order parameters ψ_{p} and ψ_{n} are defined on the gridpoints as $\psi_{\mathrm{p}}^{i,j}$ and $\psi_{\mathrm{n}}^{i,j}$, while the vector field **A** has two components, (A_x, A_y), defined on the corresponding links between the gridpoints, i.e., we have $A_x^{i+1/2,j}$ and $A_y^{i,j+1/2}$.

- The gauge coupling between ψ_{p} and **A** is implemented using a **Peierls substitution** to preserve (discrete) gauge symmetry, e.g.,

$$\left|\left(\frac{\partial}{\partial x} - \mathrm{i}A_x\right)\psi_{\mathrm{p}}\right| = \left|\frac{\partial}{\partial x}\exp(-\textstyle\int \mathrm{i}A_x\,\mathrm{d}x)\psi_{\mathrm{p}}\right|$$

$$\Rightarrow \left|\left(\frac{\partial}{\partial x} - \mathrm{i}A_x\right)\psi_{\mathrm{p}}\right|^{i+1/2,j} \simeq \frac{1}{\delta x}\left|\exp(-\mathrm{i}A_x^{i+1/2,j}\,\delta x)\psi_{\mathrm{p}}^{i+1,j} - \psi_{\mathrm{p}}^{i,j}\right| . \qquad (16)$$

- This leads to a discrete approximation $\mathcal{F}_{\mathsf{dis}}[\psi_{\mathrm{p}}^{i,j}, \psi_{\mathrm{n}}^{i,j}, A_x^{i+1/2,j}, A_y^{i,j+1/2}]$ and we obtain the ground state using a gradient-descent, iteration method.

SC formation

- In the outer core, initially, only protons are superconducting (neutrons remain normal), so we model the **formation of the superconducting phase** with a single-component time-dependent Ginzburg-Landau model.

- Study the **dynamics of the phase transition** under different circumstances in analogy to numerical experiments of laboratory systems (Liu, Mondello & Goldenfeld, 1991; Frahm, Ullah & Dorsey, 1991).

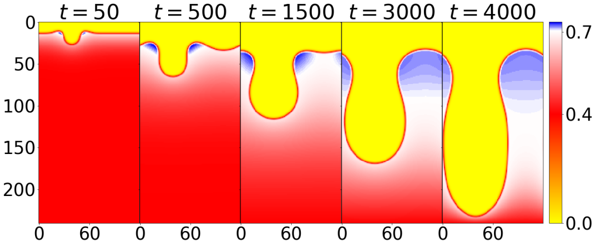

Figure 12: Evolution of the magnetic field in a type-I system in the nucleation regime.

References I

Alford M. G., Good G., 2008, Physical Review B, 78, 024510

Alpar M. A., Langer S. A., Sauls J. A., 1984, The Astrophysical Journal, 282, 533

Andersson N., Comer G., Glampedakis K., 2005, Nuclear Physics A, 763, 212

Andreev A. F., Bashkin E. P., 1975, Soviet Physics JETP, 42, 164

Bardeen J., Cooper L. N., Schrieffer J. R., 1957, Physical Review, 108, 1175

Baym G., Pethick C. J., Pines D., 1969, Nature, 224, 673

Chamel N., 2008, Monthly Notices of the Royal Astronomical Society, 388, 737

Chamel N., Haensel P., 2006, Physical Review C, 73, 045802

Charbonneau J., Zhitnitsky A. R., 2007, Physical Review C, 76, 015801

Frahm H., Ullah S., Dorsey A. T., 1991, Physical Review Letters, 66, 3067

Graber V., 2017, Astronomische Nachrichten, 338, 1090

Graber V., Andersson N., Glampedakis K., Lander S. K., 2015, Monthly Notices of the Royal Astronomical Society, 453, 671

Haber A., Schmitt A., 2017, Physical Review D, 95, 116016

Ho W. C., Glampedakis K., Andersson N., 2012, Monthly Notices of the Royal Astronomical Society, 422, 2632

Ho W. C. G., Elshamouty K. G., Heinke C. O., Potekhin A. Y., 2015, Physical Review C, 91, 015806

Ho W. W. C. G., Andersson N., Graber V., 2017, Physical Review C, 96, 065801

Kobyakov D. N., 2020, Physical Review C, 102, 045803

Liu F., Mondello M., Goldenfeld N., 1991, Physical Review Letters, 66, 3071

Migdal A. B., 1959, Nuclear Physics, 13, 655

Appendix

References II

Mösta P. et al., 2014, The Astrophysical Journal, 785, L29

Muslimov A. G., Tsygan A. I., 1985, Soviet Astronomy Letters, 11, 80

Narayan R., Ostriker J. P., 1990, The Astrophysical Journal, 352, 222

Steiner A. W., Prakash M., Lattimer J. M., Ellis P. J., 2005, Physics reports, 411, 325

Thompson C., Duncan R. C., 1995, Monthly Notices of the Royal Astronomical Society, 275, 255

Viganò D., Rea N., Pons J. A., Perna R., Aguilera D. N., Miralles J. A., 2013, Monthly Notices of the Royal Astronomical Society, 434, 123

Wood T. S., Graber V., Newton W. G., 2020, arXiv, 1

Wood T. S., Mesgarnezhad M., Stagg G. W., Barenghi C. F., 2019, Physical Review B, 100, 024505